Scientific Research Publishing

Journal of Materials Science and Chemical Engineering, 2025, 13(9), 55-66
https://www.scirp.org/journal/msce
ISSN Online: 2327-6053
ISSN Print: 2327-6045

Influence of Crystal Dimensions and P-Layer Thickness on the Optimum Doping Rate for the Best Diffusion Capacity of a Polycrystalline Solar Cell

Moussa Camara[1,2*], Moustapha Thiame[2], Issa Faye[2], Sada Traore[2], Mahamat Batran Mouta[2], Boubacar Fickou[2], Landing Diatta[2]

[1]Faculté des Sciences, Université Gamal Abdel Nasser de Conakry, Conakry, République de Guinée
[2]Département de Physique, UFR ST, Laboratoire de Chimie et de Physique des Matériaux (LCPM), Ziguinchor, Sénégal
Email: *moussounkar@gmail.com

How to cite this paper: Camara, M., Thiame, M., Faye, I., Traore, S., Mouta, M.B., Fickou, B. and Diatta, L. (2025) Influence of Crystal Dimensions and P-Layer Thickness on the Optimum Doping Rate for the Best Diffusion Capacity of a Polycrystalline Solar Cell. *Journal of Materials Science and Chemical Engineering*, **13**, 55-66.
https://doi.org/10.4236/msce.2025.139004

Received: July 31, 2025
Accepted: September 12, 2025
Published: September 15, 2025

Abstract

After three-dimensional modeling, we expressed the diffusion capacity of p-layer charges through the transition zone as a function of the impurity concentration in the p-layer, the dimensions of a polycrystalline silicon crystal, and the penetration depth of the p-layer. After analyzing the impact of the parameters cited below on the diffusion capacity, we concluded that the best diffusion capacity is obtained for a dopant range between 10^{15} and 10^{17} cm^{-3}. This range is modified by variations in crystal size and p-layer thickness. Thus, increasing crystal size shifts the optimum point towards high doping rates, while increasing p-layer thickness shifts the optimum point towards low p-layer doping rates.

Keywords

Diffusion Capacity, P-Layer, Three-Dimensional, Optimum Doping, Polycrystalline Solar Cell

1. Introduction

If we bring N-doped silicon into contact with P-doped silicon, we create a transition zone, also known as a space charge zone. From this zone, we can evaluate the carrier flux that contributes to the current produced by the silicon photovoltaic cell through charge diffusion. So, let's talk about charge diffusion capacity through the space charge zone. The diffusion capacitance of the solar cell is considered to be the capacitance resulting from the change in charge during the diffusion pro-

cess within the cell. This capacitance is mainly due to the fixed ionized charges at the junction boundaries and the diffusion process (diffusion capacitance).

Doping is one of the steps in the manufacture of polycrystalline silicon solar cells. Polycrystalline silicon is made from several silicon crystals fused together. Less expensive to produce, it has a slightly lower yield, around 14% and 18%. Compared to monocrystalline, polycrystalline has a low yield, due to the multiplicity of crystals [1] that make it up, the capture effect at the interface between two crystals [1], the size of the crystals [1] [2], recombination at the crystal joints [2]-[4], the doping rate [5] [6] and phenomenological parameters such as temperature [7]-[9], magnetic field [8], etc. The diffusion capacity of carriers across the PN junction has been the subject of much study in recent years [8] [10]-[14]. This is because it makes it possible to quantify the number of carriers involved in the current generation. Researchers have studied the effect of temperature [15], angle of incidence of illumination [16], electric field [17], magnetic field [18], emitter thickness [19] [20], wavelength [21] [22], and now the effect of crystal dimensions and the capture effect between two crystals on the optimum doping rate giving the best diffusion capacity. In this work, we will evaluate the influence of crystal size and the capture effect at interfaces on the optimal doping rate, giving the best diffusion capacity for the PN transition zone.

2. Mathematical Theories

We consider an n^+-p-p^+ type polycrystalline silicon backfield crystal (BSF) whose three-dimensional structure is given in **Figure 1**.

The working hypotheses are:

- We will neglect the contribution of the n^+-p layer to the photocurrent compared with that of the p layer.
- We have neglected the crystalline field that exists within the p-layer, as we have assumed that the solar cell is not polarized.
- The distribution is uniform along the *x* and *y* directions of the crystal, so radiation penetration occurs along *z*.
- Crystal joints are perpendicular to the n^+-p junction.

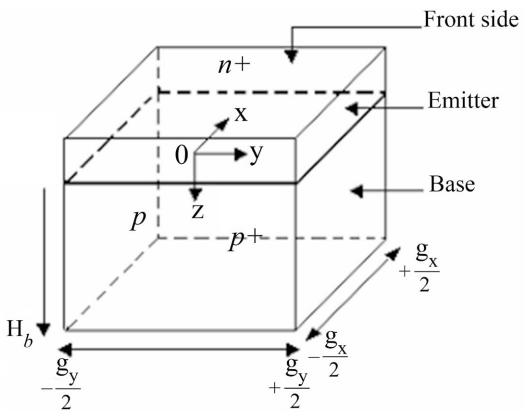

Figure 1. Example of a square crystal.

In a volume element, variations in carrier densities are caused by:

- Spontaneous generation of electron-hole pairs due to thermal agitation, characterized by the generation rate $G_n(z)$.
- Generally, assisted recombination (R_p, R_n) is usually expressed in terms of the average lifetime of minority carriers.
- Carrier flows into and out of the volume element ϕ_n.

The continuity equation, therefore, applies to charge carriers whose lifetimes are determined by recombination mechanisms in accordance with Fick's first law in the one-dimensional case:

$$\frac{\partial \delta n}{\partial t} = -div\phi_n + G_n - R_n \tag{1}$$

$$\overrightarrow{\phi_n} = -\frac{1}{e}\overrightarrow{J_n} \tag{2}$$

$$\text{Avec} \quad \overrightarrow{J_n} = en\mu_n \vec{E} + eD_n \frac{\partial \delta n}{\partial x}\vec{x} \tag{3}$$

Assuming that the solar cell is not polarized, and working in the static regime, we have obtained the simplified form of Equation (1) for a one-dimensional case:

$$0 = D_n \frac{\partial^2 \delta n}{\partial x^2} + G_n - R_n \tag{4}$$

In our work, we have generalized this one-dimensional case to obtain the three-dimensional model. This model allows us to take into account the speed of recombination at crystal boundaries. (S_{cr}). The capture effect at the interface between two crystals ($C_{kx}\, et\, C_{jy}$) and crystal dimensions (g_x, g_y). Thus, we have given the corresponding continuity equation for this model as follows [2] [23]:

$$\frac{\partial^2 \delta n(x,y,z)}{\partial x^2} + \frac{\partial^2 \delta n(x,y,z)}{\partial y^2} + \frac{\partial^2 \delta n(x,y,z)}{\partial z^2} - \frac{\delta n(x,y,z)}{Ln(Nb)} + \frac{G(z)}{Dn(Nb)} = 0 \tag{5}$$

The expression for the carrier density given by Equation (6) is the solution to Equation (5) [2] [23].

$$\delta n(x,y,z) = \sum_{kx} \sum_{jy} Z_{kx,jy} \cos(C_{kx}x)\cos(C_{jy}y) \tag{6}$$

We obtained Equation (7) by replacing the carrier density in Equation (5) with its expression given by Equation (6). With Equation (8), the solution to Equation (7) is.

$$\frac{\partial^2 Z_{kx,jy}}{\partial z^2} - \frac{1}{Ln_{kx,jy}^2} Z_{kx,jy} = \frac{1}{Dn_{kx,jy}} G(z) \tag{7}$$

$$Z_{k,j} = M_{k,j} \cos\left(\frac{z}{Ln_{k,j}(Nb)}\right) + N_{k,j} \sin\left(\frac{z}{Ln_{k,j}(Nb)}\right) - \sum_{i=1}^{3} Q_i e^{-b_i z} \tag{8}$$

$M_{k,j}$ and $N_{k,j}$ given by the boundary conditions at the surfaces bounding the p layer along the *z* axis:

- At layer n^+ or $z = 0$

$$Dn\left[\frac{\partial \delta n(x,y,z)}{z}\right]_{z=0} = Sf\,\delta n(x,y,z=0) \tag{9}$$

- At the p^+ layer or $z = H$

$$Dn\left[\frac{\partial \delta n(x,y,z=H)}{\partial z}\right]_{z=H} = -Sb\delta n(x,y,z=H) \tag{10}$$

C_k *and* C_j are obtained through crystal boundary conditions along the x and y axes:

- Following x

$$Dn\left[\frac{\partial \delta n(x,y,z)}{\partial x}\right]_{x=\pm\frac{g_x}{2}} = \mp S_{cr}\delta n\left(\pm\frac{g_x}{2},y,z\right) \tag{11}$$

- Following y

$$Dn\left[\frac{\partial \delta n(x,y,z)}{\partial z}\right]_{y=\pm\frac{g_y}{2}} = \mp S_{cr}\delta n\left(x,\pm\frac{g_y}{2},z\right) \tag{12}$$

Thus, Equation (13) gives the general equation for capacitance, and Q is the quantity of charge given by Equation (14).

$$C(x,y,z) = \frac{\partial Q(x,yx,z)}{\partial V(x,y,z)} \tag{13}$$

$$Q(x,y,z) = q\delta n(x,y,z) \tag{14}$$

$$C(x,y,z) = q\frac{\partial \delta n(x,y,z)}{\partial V} \tag{15}$$

Dividing Equation (15) by $\frac{\partial Sf}{\partial Sf}$, we have Equation (16), the solution of which gives us the capacity equation in Equation (17). $C_0(Nb)$ and $C_d\left(Nb,g_x,g_y,H\right)$ are respectively dark capacity and diffusion capacity.

$$C(x,y,z) = \frac{\partial \delta n(x,y,z)}{\partial Sf}\frac{1}{\frac{\partial V(x,y,z)}{\partial Sf}} \tag{16}$$

$$C(x,y,z) = \frac{qn_i^2}{NbV_T} + q\frac{\delta n(x,y,z=0)}{V_T} \tag{17}$$

$$C_0(Nb) = \frac{qn_i}{NbV_T} \tag{18}$$

$$C_d(x,y,Nb) = q\frac{\delta n(x,y,z=0)}{V_T} \tag{19}$$

$$C\left(g_x,g_y,Nb,H\right) = C_0(Nb) + C_d\left(Nb,g_x,g_y,H\right) \tag{20}$$

3. Results and Discussion

Influence of grain size and interface capture on the effect of doping rate on effective diffusion length

The effective diffusion length is the distance electrons have to travel before recombination, and is related to crystal size, the rate of loss at the crystal joints [1] [2], and the doping rate of the p-layer.

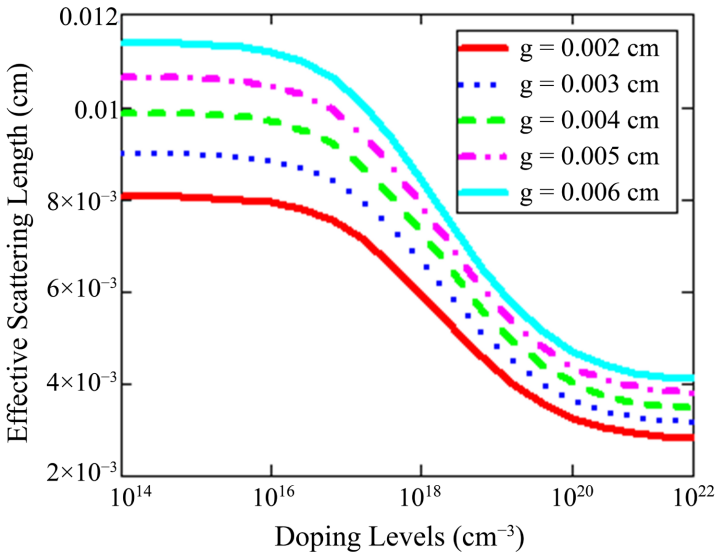

Figure 2. Profile of the effective diffusion length as a function of the proportion of base dopant for some grain size: $S_g = 10^3$ cm.s^{-1}.

To analyze the impact of the proportion of p-layer dopant on the effective diffusion length, Figure 2 shows the effective diffusion length as a function of p-layer dopant for several crystal size values along the *x* and *y* axes, respectively ($g_x = g_y = g$).

In Figure 2, we can see three zones:

A first zone for dopant levels ranging from 10^{14} cm^{-3} to 10^{15} cm^{-3} shows a plateau in effective diffusion length. In this zone, the effective diffusion length is insensitive to changes in dopant level.

A second zone for p-layer dopant levels ranging from 3.10^{15} cm^{-3} to 10^{17} cm^{-3}, the effective diffusion length decreases slightly with the dopant level. This is explained by a decrease in charge carrier lifetime with increasing p-layer dopant concentration. Increased doping, which consists of introducing impurities into silicon, increases the density of charge carriers (electrons and holes). This increase in density, in turn, promotes Auger recombination, a process whereby the energy of an electron recombining with a hole is transferred to another electron, heating it up. This phenomenon reduces the lifetime of charge carriers and decreases the likelihood of these charges being collected by the solar cell junction, resulting in a loss of power.

A third zone, from 10^{17} cm^{-3} to 10^{18} cm^{-3}, whose diffusion length decreases con-

siderably with dopant concentration, becoming constant for dopant levels above 10^{18} cm^{-3}. In this zone, the material loses its semiconducting properties and becomes a conductor.

We also analyze an increase in the effective diffusion length with increasing crystal dimensions (along *x* and *y*), as shown by Dugas and Oualid in 1987. This increase in diffusion length can be explained by the fact that increasing crystal dimensions reduces the density of recombination centers. We also note that, for low dopant concentrations (zones 1 and 2), the effective diffusion length increases strongly with crystal size. So, to obtain a better effective diffusion length, the dopant concentration must be between 10^{15} cm^{-3} and 10^{17} cm^{-3} for large grains. If the dopant concentration is higher than 10^{17} cm^{-3}, the small grains should be used.

In the following paragraph, we'll look at the impact of crystal size on the effect of p-layer dopant content on diffusion capacitance.

Influence of junction electron loss rate and low p-layer doping rates on diffusion capacity

Figure 3 shows the diffusion capacity of the solar cell as a function of the recombination velocity at the junction for different low doping levels of the p-layer.

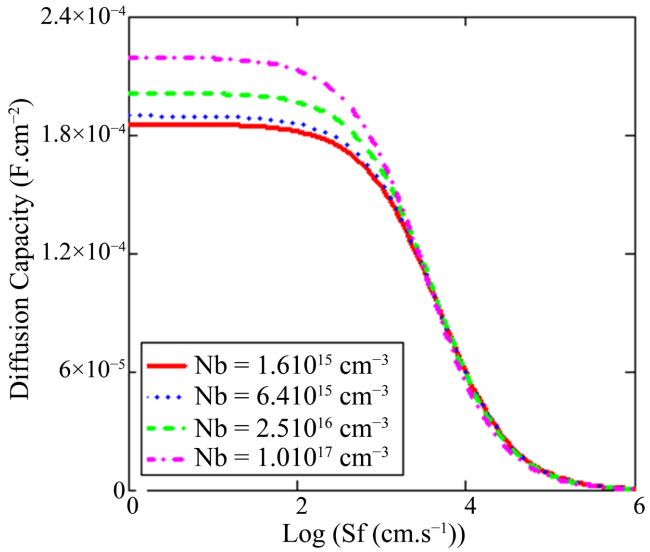

Figure 3. Diffusion capacity profile as a function of recombination velocity at the junction for low base doping levels: H_b = 120 µm, g = 64 µm, Sb = 10^4 cm/s, S_{cr} = 10^3 cm/s.

Figure 3 shows that for a given doping level, at low recombination rates at the junction, the cell's diffusion capacity is constant and corresponds to the open-circuit diffusion capacity. In an open circuit, the charge is stored on both sides of the transition zone.

At high recombination velocities at the junction, the diffusion capacity is almost zero, which corresponds to the diffusion capacity at short circuits.

We also note that the amplitude of the diffusion capacitance increases with lower p-layer doping ratios (Figure 3). Indeed, when impurities are introduced into the

p-layer, the conductivity of the semiconductor improves. The storage of minority charge carriers in the vicinity of the transition zone also increases. This is why diffusion capacity is improved in this area. This is confirmed by Figure 4, which shows that diffusion capacity increases with low doping levels.

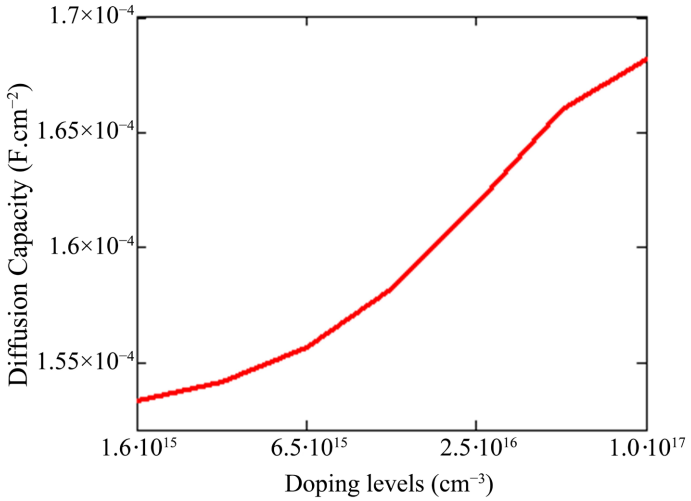

Figure 4. Diffusion capacity profile as a function of low base doping levels: H_b = 120 µm, g = 64 µm, Sb = 10^4 cm/s, S_g = 10^3 cm/s.

Intrinsic semiconductors are akin to insulators, with no free electrons to pass through them. Conduction is improved by adding a tiny amount of dopant to the intrinsic semiconductor. This process, known as doping, generates a large number of free carriers. This leads to an increase in the density of minority charges as the doping rate of the p-layer increases (from 10^{15} cm^{-3} to 10^{17} cm^{-3}), which in turn increases the diffusion capacity of the photopile Figure 3 and Figure 4.

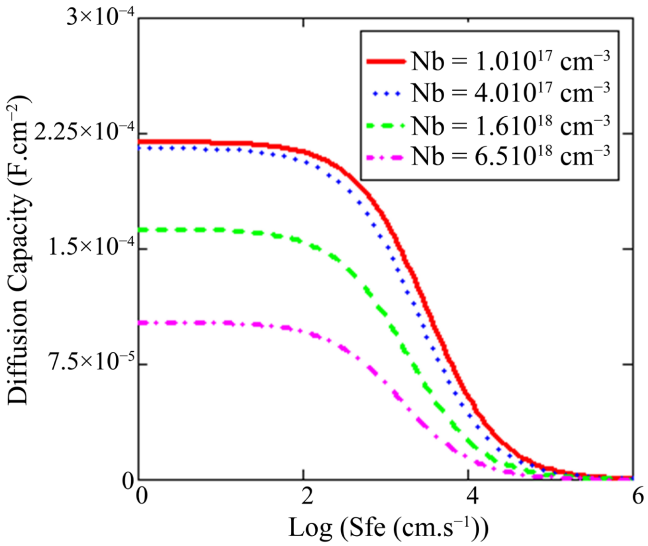

Figure 5. Diffusion capacity profile as a function of junction recombination velocity for high p-layer doping rates: H_b = 120 µm, g = 64 µm, Sb = 10^4 cm/s, S_g = 10^3 cm/s.

Influence of junction electron loss rate and high p-layer doping rates on diffusion capacity

Figure 5 shows profiles of the solar cell's diffusion capacity as a function of junction recombination velocity for high p-layer doping levels.

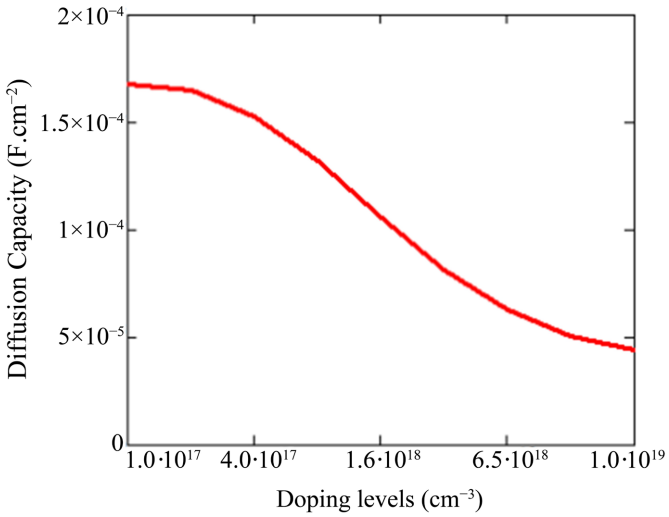

Figure 6. Diffusion capacity profile as a function of high p-layer doping rates: H_b = 120 µm, g = 64 µm, Sb = 10^4 cm/s, S_g = 10^3 cm/s.

In this section, we analyze a decrease in the diffusion capacity of the solar cell as a function of the doping rate of the p-layer for low values of the recombination velocity at the junction (Figure 5). The physical mechanism related to energy band boundary deformation is associated with free donor-transporter interactions. These interactions increase the initially discrete impurity level. This leads to the union of this energy band of excess ionized impurities with the valence band.

In heavily doped silicon, the mechanism linked to the distortion of energy band boundaries can be summarized in three cases:

- The limits of the valence and conduction bands give rise to tails that penetrate the band gap.
- If the rate of acceptor dopants is high, the energy levels of the dopants expand into a dopant band that overlaps with the valence band.
- A high number of acceptor atoms leads to a spatial variation in bandgap width, resulting in crystal lattice deformation.

These changes result in an apparent drop in bandgap width. This leads to a reduction in storage diffusion capacity at high impurity levels Figure 5 and Figure 6.

The doping of semiconductor substrates allows us to vary their electrical conductivity over a wide range. Highly doped semiconductors (n^+ or p^+) have a conductivity close to that of metals. This leads to a reduction in diffusion capacity. These are the areas we encounter when making ohmic contacts.

By analyzing Figure 3, Figure 4, Figure 5, and Figure 6, we obtain an optimum

value for the p-layer dopant ratio of the order of 10^{17} cm^{-3}. In the next paragraph, we'll look at the impact of crystal size and p-layer thickness on this optimum value for impurity concentration.

Influence of crystal dimensions and p-layer thickness on the optimum doping rate for best diffusion capability.

Figure 7 and Figure 8 show the diffusion capacity profile of the photovoltaic cell as a function of the doping rate of the p-layer, respectively, for different sizes of the crystal and thicknesses of the p-layer.

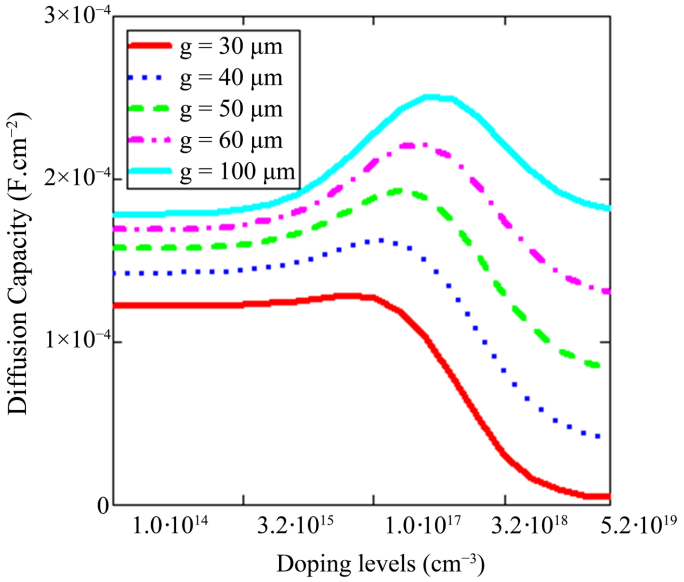

Figure 7. Capacitance profile as a function of base doping rate for various crystal sizes and p-layer thicknesses, respectively: g = 64 µm, Sb = 10^3 cm/s, S_{cr} = 10^3 cm/s, and H_b = 120 µm.

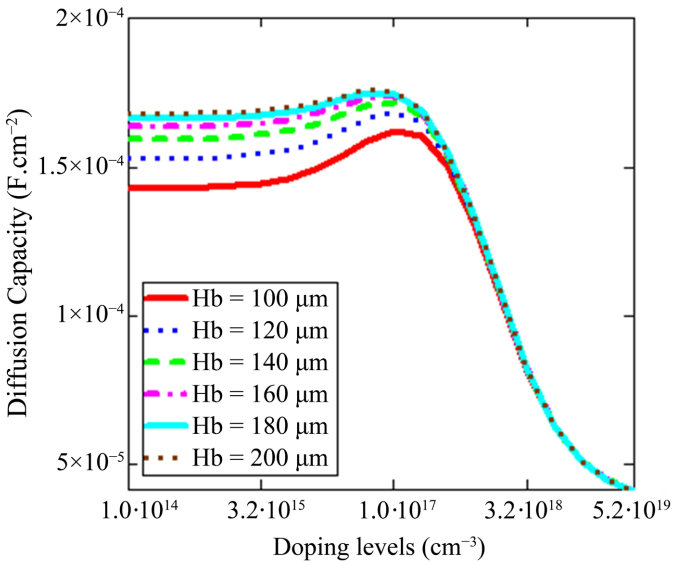

Figure 8. Capacitance profile as a function of base doping rate for various p-layer thicknesses, respectively: g = 64 µm, Sb = 10^3 cm/s, S_{cr} = 10^3 cm/s.

The figures above show that the cell's capacity increases with crystal size along the *x* and *y* axes (Figure 7), and with p-layer thickness along the *z* axis (Figure 8).

This increase is explained by the growth of minority carriers as the dimensions of Figure 7 and the thickness of the p-layer in Figure 8 increase. Crystalline silicon is characterized by broad absorption over the entire solar spectrum. However, the absorption coefficients associated with these wavelengths are low. Silicon solar cells would need to be several tens of microns thick to absorb the light. As a result, the effect of minority carriers is accentuated in larger and thicker solar cells, as the larger volume of the base results in a greater number of minority carriers in the p-layer.

Figure 7 shows that increasing the dimensions along *x* and *y* increases the optimum doping rate, while increasing the p-layer thickness decreases the optimum p-layer doping rate Figure 8. In other words, the larger the crystal dimensions along x and y and the smaller the p-layer thickness, the higher the optimum p-layer doping rate.

4. Conclusion

In this work, we have shown that the maximum diffusion capacity is obtained for p-layer dopant concentrations between 10^{15} cm^{-3} and $10^{17}cm^{-3}$. We then studied the effect of crystal dimensions and p-layer dopant penetration depth on the optimum impurity ratio, which gave the best diffusion capacity. From our analysis, we found that the amount of dopant giving the best diffusion capacity (the diffusion capacity corresponding to the optimum doping rate) increases with crystal size, whereas it decreases with increasing impurity penetration depth.

Conflicts of Interest

The authors declare no conflicts of interest regarding the publication of this paper.

References

[1] Camara, M., Toure, M., Siba, H., Mouta, M.B., Camara, O.F. and Thiame, M. (2025) Analyse of Impact of Temperature, Grain Sise and Magnetic Field on Effective Diffusion Length. *Asian Journal of Science and Technology*, **16**, 13516-13519.

[2] Diallo, H.L., Seïdou Maiga, A., Wereme, A. and Sissoko, G. (2008) New Approach of Both Junction and Back Surface Recombination Velocities in a 3D Modelling Study of a Polycrystalline Silicon Solar Cell. *The European Physical Journal Applied Physics*, **42**, 203-211. https://doi.org/10.1051/epjap:2008085

[3] Barro, F.I., Ndiaye, M., Deme, M., Mbodji, S., Ba, E. and Sissoko, G. (2008) Influence of Grains Size and Grains Boundaries Recombinaison on the Space-Charge Layer Thickness z of Emitter Base Junction's n^+-p-p^+ Solar Cell. *Proceedings of the* 23*rd European Photovaltaic Solar Energy Conference and Exhibition*, Valencia, 1-5 September 2008, 608-611.

[4] Mbodji, S., Ly, I., Diallo, H.L., Dione, M.M., Diasse, O. and Sissoko, G. (2012) Modeling Study of N^+/P Solar Cell Resistances from Single I-V Charactristic Cuve Considering the Junction Recombiation Velocity (Sf). *Research Journal of Applied Science, Engineering and Technology*, **4**, 1-7.

[5] Traore, S., Diedhiou, A. and Ndiaye, M. (2024) Study of the Performance Parameters of a Silicon Solar Cell ($n^+/p/p^+$) in Frequency Modulation Placed in a Medium Dominated by the Magnetic Field: Effect of Low and High Doping Rate. *Journal of Engineering and Technology*, **16**, 24-28.

[6] Thiame, M., Camara, M., Lemrabott, H., Lemine Cheikh, M., Gueye, S. and Sissoko, G. (2023) Etude A 3d de la Photopile au Silicium Polycristallin: Optimisation du Taux de Dopage en Fonction de Lepaisseur de la Base. *International Journal of Advanced Research*, **11**, 311-322. https://doi.org/10.21474/ijar01/17989

[7] Traore, S., Diedhiou, A., Sambou, A. and Camara, M. (2024) Study of the Electrical Parameters of a Silicon Solar Cell ($n^+/p/p^+$) under the Effect of Temperature by Optimization of the Base Thickness and the Doping Rate. *Journal of Materials Science and Chemical Engineering*, **12**, 15-23. https://doi.org/10.4236/msce.2024.1211002

[8] Camara, M., Thiame, M., Toure, M., Siba, H. and Fanta Camara, O. (2025) Effect of Crystal Size on the Optimum Temperature for the Highest Capacity of a Tree-Dimensional Polycrystalline Silicon Solar Cell. *International Journal of Advanced Research*, **13**, 443-452. https://doi.org/10.21474/ijar01/20215

[9] Diatta, I., Diagne, I., Sarr, C., Faye, K., Ndiaye, M. and Sissoko, G. (2015) Silicon Solar Cell Capacitance: Influence of Both Temperature and Wavelength. *International Journal of Computer Science*, **3**, 1-8.

[10] Böer, K.W. (2010) Introduction to Space Charge Effects in Semiconductors. Springer.

[11] Khan, R. and Faiz, W.U. (2021) Comparative Analysis of Capacitance Finding Techniques of a Solar Cell. *International Journal of Engineering Works*, **8**, 85-92. https://doi.org/10.34259/ijew.21.8038592

[12] Yaron, G. and Frohman-Bentchkowsky, D. (1980) Capacitance Voltage Characterization of Poly Si-SiO_2-Si Structures. *Solid-State Electronics*, **23**, 433-439. https://doi.org/10.1016/0038-1101(80)90078-7

[13] Sissoko, G., Dieng, B., Corréa, A., Adj, M. and Azilinon, D. (2004) Silicon Solar Cell Space Charge Region Width Determination by a Study in Modeling. *Renewable Energy*, **3**, 1852-1855.

[14] Chawla, B.R. and Gummel, H.K. (1971) Transition Region Capacitance of Diffused P-N Junctions. *IEEE Transactions on Electron Devices*, **18**, 178-195. https://doi.org/10.1109/t-ed.1971.17172

[15] Diatta, I., Ly, I., Wade, M., Diouf, M.S., *et al.* (2016) Temperature Effect of Capacitance Silicon Solar Cell under Constant White Biased Light. *World Journal of Condensed Matter Physics*, **6**, 261-268.

[16] Thiam, A., Zoungrana, M., Diallo, H.L., Diao, A., Thiam, N., Gueye, S., *et al.* (2013) Influence of Incident Illumination Angle on Capacitance of a Silicon Solar Cell under Frequency Modulation. *Research Journal of Applied Sciences, Engineering and Technology*, **5**, 1123-1128. https://doi.org/10.19026/rjaset.5.4825

[17] Ouedraogo, A., Ouedraogo, B., Kaboré, B. and Bathiebo, D.J. (2020) Polycrystalline Silicon Solar Cell P-N Junction Capacitance Behavior Modelling under an Integrated External Electrical Field Source in Solar Cell System. *Energy and Power Engineering*, **12**, 143-153. https://doi.org/10.4236/epe.2020.125011

[18] Boiro, M., Dione, B., Toure, I., Ndiaye, A. and Diao, A. (2022) Influence of the Magnetic Field on the Diffusion Capacitance of a Serial Vertical Junction Silicon Solar Cell in Frequency Modulation. *American Journal of Modern Physics*, **11**, 1-6. https://doi.org/10.11648/j.ajmp.20221101.11

[19] Mbodji, S., Mbow, B., Barro, F.I. and Sissoko, G. (2011) A 3D Model for Thickness

and Diffusion Capacitance of Emitter-Base Junction Determination in a Bifacial Polycrystalline Solar Cell under Real Operating Condition. *Turkish Journal of Physics*, **35**, 281-291. https://doi.org/10.3906/fiz-0911-25

[20] Mbodji, S., Mbow, M., Barro, F.I. and Sissoko, G. (2010) A 3D Model for Thickness and Diffusion Capacitance of Emitter-Base Junction in a Bifacial Polycrystalline Solar Cell. *Global Journal of Pure and Applied Sciences*, **16**, 469-477.

[21] Souleymane Dia, F., Dieng, A.B., Mbodj, S., Tabara Sow, P.L. and Sissoko, G. (2018) Wavelength's Effects on Recombination Velocities and on Diffusion Capacitance Efficiency. *International Journal of Research in Engineering and Technology*, **7**, 39-43. https://doi.org/10.15623/ijret.2018.0701008

[22] Boiro, M., Diao, A., Ndiaye, A. and Gackou, D. (2024) Influence of Wavelength on the Diffusion Capacitance of a Serial Vertical Junction Silicon Solar Cell in Frequency Regime. *American Journal of Materials Science and Engineering*, **12**, 25-29. https://doi.org/10.12691/ajmse-12-2-1

[23] Dugas, J. (1994) 3D Modelling of a Reverse Cell Made with Improved Multicrystalline Silicon Wafers. *Solar Energy Materials and Solar Cells*, **32**, 71-88. https://doi.org/10.1016/0927-0248(94)90257-7